Development of the Powertrain System for a Shell Eco-marathon Fuel Cell Electric Vehicle:

António Líbano Monteiro
antonio.libano.monteiro@tecnico.ulisboa.pt
Instituto Superior Técnico, Universidade de Lisboa, Portugal
October 2021

Abstract

In modern societies, the transport sector is highly developed and is expected to continue growing; good news for the economy, but a real threat to the environment on account of the sector being heavily dependent on fossil fuels. This is where hydrogen can play fundamental role in decarbonizing transport as a green fuel for alternative sustainable transport methods like fuel cell electric vehicles.

The main goal of this work is the design of an efficient powertrain for a hydrogen fuel cell electric vehicle as well as the development of a method for generating fuel efficient driving strategies around any track. This work is integrated in a larger student's project called Técnico Fuel Cell that aims to promote alternative ways of sustainable transportation with the design and manufacture of a small urban vehicle to compete in the Shell Eco-marathon, one of the world's most renowned energy efficiency competitions.

The backbone of the work developed in this dissertation is a computational model programmed in MATLAB to accurately simulate the vehicle's behaviour around a selected circuit. This model is then used with a genetic algorithm to optimize the powertrain design and the driving strategy specifically for the vehicle and the track characteristics, so that maximum fuel efficiency is achieved. With this method, considering a vehicle with conservative specifications compared to the other teams in terms weight, aerodynamics and efficiency of the components, a fuel efficiency of 370.2 km/m^3 of hydrogen (1208 km/L of gasoline equivalent) was simulated for the competition's 2016 London track – just 5% less than that year's overwhelming winning result, which was 39% higher than the second place. This result demonstrates the capabilities of the developed optimization method and highlights the importance of such models in the development process of the current and future vehicles of Técnico Fuel Cell.

Keywords: fuel cell electric vehicle; vehicle model; powertrain design; driving strategy; energy efficiency optimization; Shell Eco marathon.

1 Introduction

The work presented in this article aims to develop the powertrain of a high efficiency hydrogen fuel cell electric vehicle to compete with the best teams of Shell Eco-marathon (SEM). To achieve this goal, the work was divided in four major goals:

1) The development of a detailed model of the vehicle that accurately simulates its behaviour on a track;

2) The creation of a method to develop a fuel-efficient driving strategy around the selected track;

3) The design of the best and most efficient powertrain possible, using the tools previously developed;

4) To develop a sensitivity analysis of the fuel efficiency to highlight where the efforts should be focused on to further optimize the vehicle in future works.

To achieve the proposed objectives, a comprehensive research was developed on the basic principles and knowledge critical to the quality and the scientific rigour of the work developed in the article.

Shell Eco-marathon is one of the world's most renowned energy efficiency competitions. It is a unique global programme where teams of students of science, technology, engineering and maths build their own vehicles and compete against similar teams from all around the world for the highest energy efficiency.

The main Shell Eco-marathon competition for all classes is "The Mileage Challenge". The goal is to achieve a valid run using the least amount of energy and, for Urban Concepts (the class Técnico Fuel Cell is competing in), the challenge is also focused on "stop and go" driving. Therefore, vehicles competing in this class are required to do a full stop per lap and resume driving, unaided.

The SEM track routes are usually completely different from year to year. For this reason, it is impossible to know which circuit the team's vehicle will have to face and, consequently, what the powertrain will have to be capable of. To tackle this uncertainty, the London 2016 route was selected, as it is one of the most demanding circuits Shell Eco-marathon has ever taken place in, guaranteeing that the vehicle will be capable of handling any race track.

2 Vehicle Dynamics

The subject of "vehicle dynamics" is the study of the movements of vehicles on a road surface, where the motions of interest are acceleration, braking, ride and turning. The dynamic behaviour is determined by studying the forces that are imposed on the vehicle and its components with the purpose of predicting the resulting response. The forces acting on the vehicle can be narrowed down to three sources: the tires, gravity and aerodynamics.

2.1 Free-body Diagram

The first step for analysing the vehicle's dynamics is the sketching of its free body diagram, along with all the significant forces acting on it under arbitrary conditions, as seen in Figure 2.1.

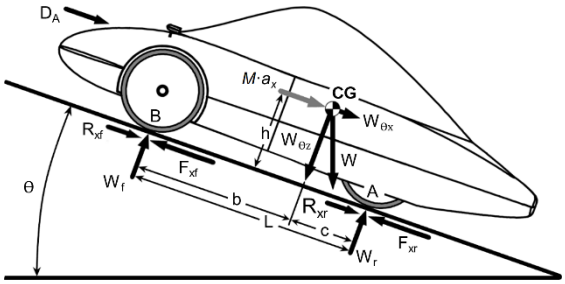

Figure 2.1 - Arbitrary forces acting on the vehicle, x-z plane.

W	-	Weight of the vehicle at its CG;
$W_{r,l}$	-	Dynamic weights of the axles experienced by the tires on the contact patches A and B;
F_x	-	Tractive force of the tires;
R_x	-	Rolling resistance of the tires;
D_a	-	Aerodynamic drag force acting on the vehicle;
$M \cdot a_x$	-	Inertial force caused by the acceleration of the vehicle, a_x, where M is the vehicle mass;
θ	-	Grande angle of the road;
L and h	-	Wheelbase and height of the CG, respectively;
c and b	-	Distance of CG from the rear and front axles.

2.2 Longitudinal Vehicle Model

In reality, vehicles not only travel on level roads but also up and down slopes and around corners. To model the vehicle's motion, a simpler straight two-dimensional road where there are no corners can be considered [1]. This is done by applying Newton's Second Law along the longitudinal axis of the vehicle (Figure 2.1), resulting in the equilibrium presented in equation (2.1):

$$F_x - (R_x + W_{\theta x} + D_A) = M \cdot \alpha_x \qquad (2.1)$$

where the rolling resistance and the tractive force are the sum of the forces for the front and rear tires.

2.2.1 Tractive Force

The tractive force generated by the electric motor can be used for accelerating or braking the vehicle. For the case where the motor "pushes" the vehicle forward, the tractive force can be determined with equation (2.2):

$$F_x = \frac{T_M \cdot N_t \cdot \eta_t}{r} - [(J_M + J_t)N_t^2 + J_w]\frac{a_x}{r^2} \qquad (2.2)$$

where:

T_M	-	Torque output of the motor [N·m];
N_t	-	Numerical gear ratio of the transmission;
η_t	-	Efficiency of the transmission;
r	-	Radius of the tires [m];
J_M	-	Rotational inertia of the motor shaft [kg·m^2];
J_t	-	Rotational inertia of the transmission (as seen from the motor side);
J_w	-	Rotational inertia of the wheels and axles;

To determine the maximum tire traction available for a rear-wheel-drive vehicle, first the dynamic weight on the rear axle must be calculated with equation (2.3):

$$W_r = W\cos\theta\frac{b}{L} + (D_a + W\sin\theta + M \cdot a_x)\frac{h}{L} \qquad (2.3)$$

after that, equation (2.4) can be applied:

$$F_{x_{max}} = \mu_t \cdot \frac{W_r}{0.5 \cdot N_w} \qquad (2.4)$$

where μ_t is the friction coefficient between the road surface and the tires and N_w is the number of wheels doing the work. The friction coefficient depends heavily on the tire characteristics, type of road surface and road conditions. However, since the vehicle is to be used only in concrete or asphalt roads, the conservative values of 0.8 and 0.5 will be used for dry and wet roads, respectively.

2.2.2 Grading Force

The grading force opposes forward motion when the vehicle is climbing and aids it when it is descending, as described by equation (2.5):

$$W_{\theta x} = W \cdot \sin\theta = mg \cdot \sin\theta \qquad (2.5)$$

2.2.3 Aerodynamic Drag

To determine the force caused by aerodynamic drag it is necessary to use a semi-empirical model because, even in the simplest of cases, the flow around a body is extremely complex. Therefore, equation (2.6) is commonly used to characterize the aerodynamic drag:

$$D_A = \frac{1}{2}\rho \cdot {v_f}^2 \cdot C_D \cdot A_F \qquad (2.6)$$

where:

C_D	-	Aerodynamic drag coefficient;
A_F	-	Frontal area of the vehicle;
v_f	-	Relative velocity of the air flow;
ρ	-	Air density.

2.2.4 Tire Drag

To model the rolling resistance drag of the tires on a straight line, equation (2.7) is commonly used:

$$R_x = f_r \cdot W \cdot \cos\theta \qquad (2.7)$$

where f_r is the rolling resistance coefficient.

However, this equation does not account for the drag caused by the tires in the corners of the track, which can be several times higher than the "straight-line" rolling resistance given by Eq. (2.7).

The increase in tire drag when cornering at higher than "parking lot" speeds occurs due to the lateral acceleration that is present when cornering which must be counteracted by the lateral forces developed by the tires. Consequently, a slip-angle appears at each tire making the lateral force contribute to the overall tire drag.

To estimate the tire drag when cornering, an adaptation of the bi-cycle model described in [2] was used to simulate the four-wheel vehicle discussed in this article. This model can be used because the turn radius is always much larger than the track width, thus, the left and right wheel steer angles can be substituted by their average and the front and rear wheels can be represented by one wheel per axle, placed in the vehicle's longitudinal plane of symmetry.

In Figure 2.2, the tire drag that results from the bi-cycle model, for various vehicle velocities and turn radii, are presented for a 170 kg vehicle (including driver) equipped with low rolling resistance Michelin Urban Concept tires.

The aerodynamic drag curve for a vehicle with a frontal area of 0.9 m^2 and an aerodynamic drag coefficient of 0.18 is also shown for comparison (dashed line).

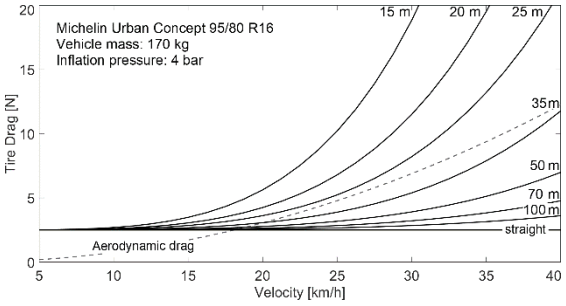

Figure 2.2 - Tire drag given by the bi-cycle model for different speeds and turn radii.

The results of the bi-cycle model clearly show that the tire drag is much higher when cornering than when moving in a straight line. In fact, for a velocity of 35 km/h a turn radius of only 50 m doubles the drag force produced by the tires, when comparing to a straight road.

2.3 Electric Motor Energy Consumption

To estimate the energy consumption of the vehicle, an appropriate model of the electric motor must be used. The model is fundamental to establish the relationship between the rotational mechanical energy of the drive system and the electrical energy of the powertrain. However, since different machines require different models to simulate how they work, it is necessary to first determine the motor technology to be used. To do this, the Multi-Criteria Decision Making (MCDM) Table 2.1 was built to assist with the selection of the best motor technology for the vehicle. The selected criteria values for each motor type were selected based on the comparison of datasheets from real motors and on the references [3]–[6].

Table 2.1 - Multi-Criteria Decision Making table for the selection of motor technologies.

Criteria		**Type of Motor**				
	wt.[1]	**DC**	**IM**	**RM**	**BLDC**	**PMSM**
Efficiency	5	1	2	3	4	5
Power Density	4	2	3	3	4	5
Control Complexity	3	5	2	4	4	2
Cost	2	4	5	4	3	1
Maintenance	1	1	5	5	5	5
	Score:	37	43	52	**59**	58

[1] Weight of each criterion (1 – Not Important to 5 – Very Important).
* Criteria are evaluated from 1 – Poor to 5 – Excellent.
* DC – Brushed DC; IM – Induction Motor; RM – Reluctance Motor; BLDC – Brushless DC; PMSM – Permanent Magnet Synchronous Motor

Based on the scores from Table 2.1, the type of motor that was selected is of the brushless DC technology. However, it should be noted that the PMSM also had a very high rating and, if cost is disregarded, it even surpasses the BLDC as the best choice for the vehicle.

To model the BLDC motor, the modified constant current model (MCCM) proposed by Prof. K. Krykowski in [7] was used. The MCCM has the advantage of being a simple functional model that estimates the relationships between current, voltage, load torque and rotational speeds, while also taking into account the impact of inductance on the torque speed characteristics of the BLDC motor.

The main values to be obtained from the model are the load torque, used for equation (2.2), and the input voltage U_d that, multiplied with the input current, gives the motor input power.

The efficiency of the BG 95x80 dCore BLDC motor is shown in Figure 2.3, simulated with the MCCM.

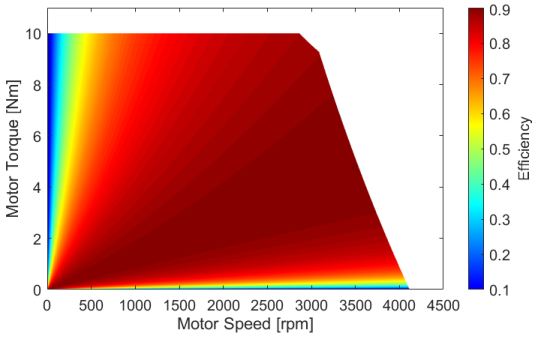

Figure 2.3 - Efficiency map of a BG 95x80 dCore BLDC motor.

One value that was not given in the motor's datasheet [8] and had to be estimated was motor's viscous damping coefficient. This can be done with equation (2.8) which ensures that, in no load conditions, a current equal to the no-load current I_{nl} is consumed when the motor is rotating at the no-load speed ω_{nl} [9]:

$$B = \frac{K_t \cdot I_{nl}}{\omega_{nl}} \tag{2.8}$$

where K_t is the torque constant given by the manufacturer.

The values simulated by the model for the nominal and no-load rotational speeds are equal to: K_n = 3806 rpm and K_{nl} = 4116 rpm. These values differ from those given in the motor's data sheet by approximately 2% and 1%, respectively, which shows that the model gives a good approximation of the real motor operation.

In Figure 2.3, it can be observed that the efficiencies predicted by the model for very low torques and speeds are not accurate. This can result from it not including other types of energy loss like eddy current and hysteresis losses, which could contribute to decrease the efficiency for these working conditions. However, in the vehicle's case, the motor should operate at close to nominal torques and speeds most of the time, where the model is most accurate. Even so, the author recommends that a comprehensive study of the acquired electric motor is done in a testbench to obtain the characteristic curves and parameters of the motor, so the model can be validated and fine-tuned if needed.

3 Vehicle Model

The vehicle model was developed using MATLAB's scripts and functions, instead of the more user-friendly Simulink. This decision was made to keep the model simple and its computing time fast, to later use heuristic optimization algorithms to find an optimal solution for the driving strategy. It was assumed that using these algorithms with Simulink would be too time consuming.

The simulation is split in two models: the main one simulates everything from the motor to the wheel and is responsible for calculating the velocity profile of the vehicle, as well as estimating the energy consumed by the electric motor; the second model runs together with the main model, receiving data from it to simulate the rest of the powertrain, from the fuel cell to the motor, and estimate the hydrogen consumption.

3.1 Model Assumptions

Other than the assumptions already mentioned in Section 2, several other simplifications were made to avoid needlessly overcomplicating the model, delivering easier to interpret results and faster simulation running times.

The assumptions used are divided in two parts; one for the vehicle system and control and the other for the racetrack and other external factors:

Vehicle:

a. The driver perfectly executes the driving plan;
b. The powertrain always provides the necessary current-voltage conditions for the electric motor;
c. The rolling resistance coefficient is constant;
d. Iterations are calculated in steps of one metre and all the variables and conditions are constant in each iteration;
e. The motor current control is perfect.

Track:

f. Only one lap around the track is simulated;
g. The track is treated in discrete steps of one metre;
h. The atmospheric conditions are constant at standard sea-level pressure (1 atm) and 15 ºC;
i. The road surface is dry;
j. Negligible wind;
k. Smooth road surface and in good condition.

3.2 Vehicle Dynamics Model

Knowing the motor input current at every point of the track, the main variable that is carried over between iterations is the vehicle velocity, i.e., the final velocity of one iteration is the initial of the next. The final lap time and energy consumption are calculated summing the time and energy consumed of all segments of the track.

After defining the duty cycle strategy, i.e., the input current along the track, the model follows the flowchart diagram shown in Figure 3.1.

To calculate acceleration of the vehicle, equations (2.1) and (2.2) are combined, resulting in equation (3.1):

$$a_x = \frac{T_M \cdot N_t \cdot \eta_t \cdot \frac{1}{r} - (R_x + W_{\theta x} + D_A)}{M + [(J_M + J_t)N_t^2 + J_w] \cdot \frac{1}{r^2}} \quad (3.1)$$

The final velocity and the time interval of each iteration can be determined with the third and first equations of motion, Eq. (3.2) and Eq. (3.3), respectively:

$$v_{i+1} = \sqrt{v_i^2 + 2 \cdot a_x \cdot \Delta x} \quad (3.2)$$

$$\Delta t_i = \frac{v_{i+1} - v_i}{a_x} \quad (3.3)$$

Considering that for any segment (i to i+1), the power versus time plot has a trapezoidal shape, the energy consumed by the motor per iteration, $E_{M,i}$, can be calculated with equation (3.4):

$$E_{M,i} = \frac{1}{2}\left(P_{M,i} + P_{M,i+1}\right) \cdot \Delta t_i \quad (3.4)$$

Finally, the energy consumed by the motor and the lap time are determined by summing the values calculated for all iterations:

$$E_M = \sum_{i=1}^{x_{lap}} E_{M,i} \quad (3.5)$$

$$t_{lap} = \sum_{i=1}^{x_{lap}} \Delta t_i \quad (3.6)$$

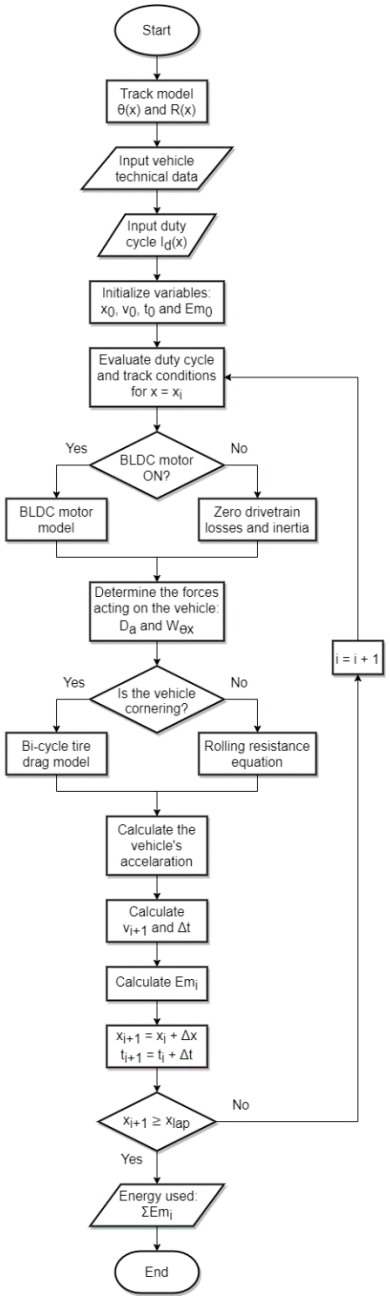

Figure 3.1 - Flowchart of the vehicle's simulation algorithm.

For faster simulation computational times, the bi-cycle model was pre-mapped to avoid having to solve it during the simulation. Doing this enabled the simulation to run around 10 times faster than when the full bi-cycle model was solved and resulted in the map shown in Figure 3.2.

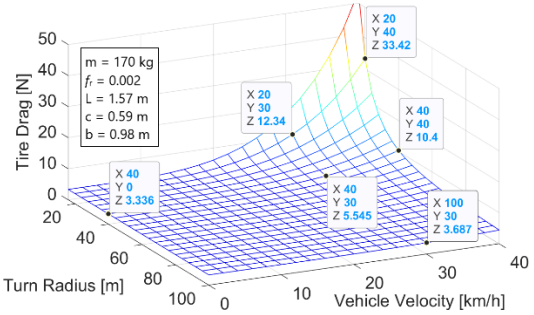

Figure 3.2 - Tire Drag Map

3.3 Vehicle Fuel Cell to Motor Models

This section describes two fuel cell to motor models and their implementation with the model of Section 3.2.

The FC-motor model is what closes the gap between the hydrogen consumption, which is ultimately what is to be minimized, and the motor to wheel model. The FC-motor models run in parallel with the motor to wheel model, as they use the data provided for the motor energy consumption and input power to calculate the energy output and hydrogen consumption of the fuel cell.

3.3.1 Parallel Active Hybrid Model

The use of a supercapacitor (SC) creates the need for a control strategy to dictate the flow of energy. For this model, the control of the energy flow is driven by the energy consumed and the average input power of the electric motor, as well as the state of charge (SOC) of the supercapacitor, at each iteration.

The schematic of the energy flow for the parallel active hybrid powertrain configuration is shown in Figure 3.3.

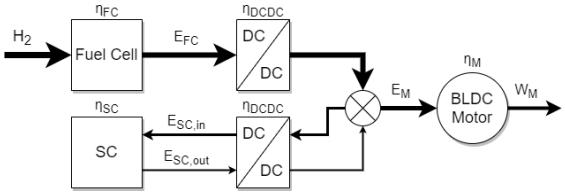

Figure 3.3 - Parallel active hybrid model energy flow.

Following the direction of the energy flow arrows, the equations that describe this model are:

$$E_{FC,i} = E_{H_2,i} \cdot \eta_{FC}(P_{FC,i}) \quad (3.7)$$

$$E_{SC,i+1} = E_{SC,i} + E_{SC_{in},i} \cdot \eta_{SC} - E_{SC_{out},i} \quad (3.8)$$

$$\eta_{DCDC} \cdot \left(E_{FC,i} + E_{SC_{out},i}\right) - E_{M,i} - \frac{E_{SC_{in},i}}{\eta_{DCDC}} = 0 \quad (3.9)$$

The control strategy shown in the flowchart of Figure 3.4 was developed to simulate the behaviour of the powertrain as it responds to the change in the power requested by the electric motor. The main goal of this control strategy is to maintain the power output of the fuel cell constant at its maximum efficiency operating point and also to guarantee that the SOC of the supercapacitor ends the lap at a value equal or slightly above the value at the beginning of the lap. This requirement comes from a rule of the competition which states that the SOC of the SC at the end of the full run must be equal or higher than at the start of the run [10].

The simulation of the fuel cell to motor model runs without known values for the energy storage capacity of the SC. Hence, the minimum specifications of the SC are also an output of this model. This is achieved by starting the simulation with a symbolic value of zero for the energy stored in the SC. Then, as the simulation progresses, the maximum (positive) and minimum (negative) values of the energy stored in the supercapacitor are registered and the minimum required capacity is calculated according to equation (3.10), which assumes a 75% capacity usage [11].

$$E_{SC_{max}} - E_{SC_{min}} = 0.75 \cdot \frac{1}{2} \cdot C \cdot {V_{SC_{max}}}^2 \quad (3.10)$$

where:

C - Capacitance of the SC in Faraday;

$V_{SC_{max}}$ - Maximum voltage of the SC;

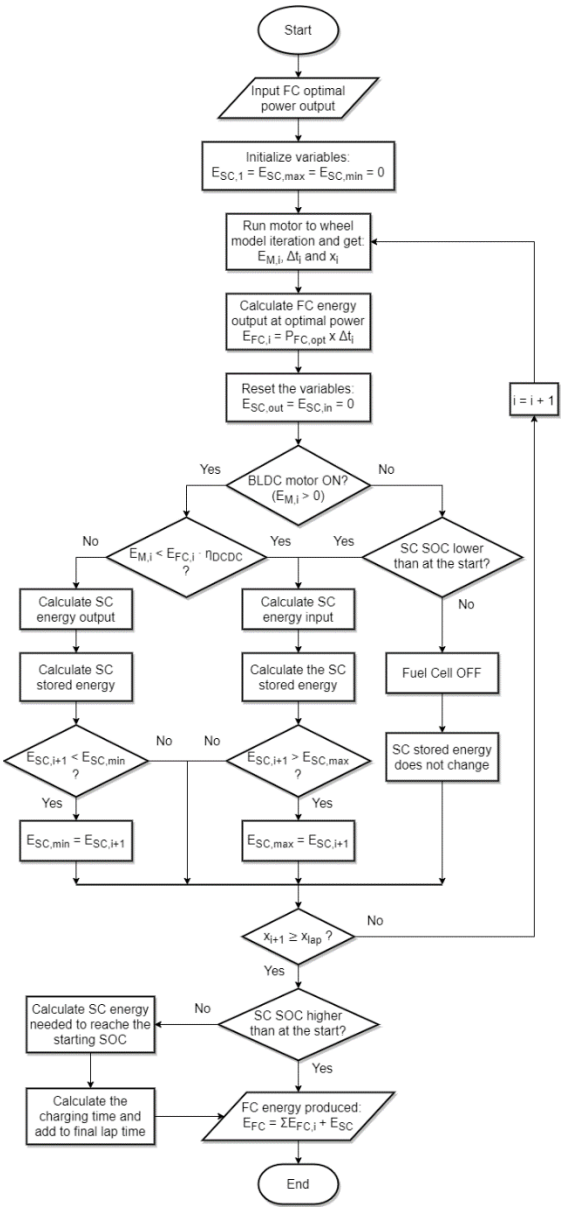

Figure 3.4 - Flowchart of the parallel active hybrid model.

3.3.2 Fuel Cell Active Model

This model is simple and straightforward; it is equivalent to the parallel active hybrid model without the supercapacitor branch. Hence, the equations that describe this model are Eq. (3.7) and Eq. (3.9), with the supercapacitor variables ($E_{SC_{in},i}$ and $E_{SC_{out},i}$) equal to 0.

3.3.3 Fuel Cell Efficiency

For the fuel cell efficiency, the values provided by the manufacturer were used because no mathematical model of the fuel cell was developed.

The used fuel cell hydrogen conversion efficiency, shown in Figure 3.5, was extracted from the "average fuel consumption" values (blue line) given by the manufacturer in the fuel cell's manual [12].

The hydrogen consumed by the fuel cell can be easily converted from Joules to kg or m^3 with the net calorific value (NCV) and density for hydrogen at 15 ºC and 1 atm.

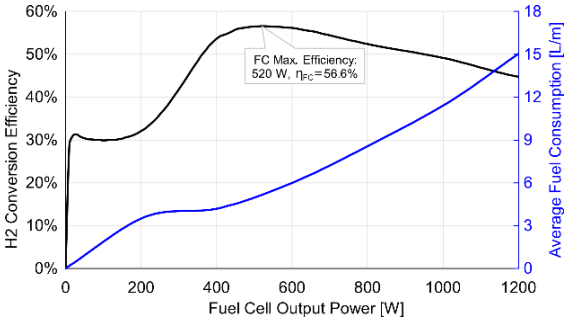

Figure 3.5 - Horizon H-1000XP fuel cell performance.

4 Driving Strategy and Powertrain Design

The optimization of the mission the vehicle is designed to complete is one of the most important steps to achieve the best possible performance. Even the most optimized and fine-tuned vehicle imaginable will perform poorly if the driving strategy is inadequate.

4.1 Optimization Problem

Considering that the prime goal of the Shell Eco-marathon competition is to achieve maximum energy efficiency, the hydrogen consumption of the fuel cell E_{H_2} was selected as the objective function to be minimized. Therefore, the discrete optimization problem (OP) used with the models developed in this work can be written as:

$$\min_{I_{d_i}} E_{H_2}(I_{d_i}) \tag{4.1}$$

s.t.

$$t_i \in [0, t_{lap}^{max}] \tag{4.2}$$

$$v_i \in [0, v^{max}] \tag{4.3}$$

$$|F_{x_i}| \leq F_x^{max}(W_{r_i}) \tag{4.4}$$

$$|I_{d_i}| \leq I_d^{max}(v_i) \tag{4.5}$$

where constraints (4.2) and (4.3) come from the maximum time for the attempt and the maximum velocity allowed by the rules, respectively; constraint (4.4) from the maximum traction available at the tires; and constraint (4.5) from the motor maximum input current.

Finally, depending on which powertrain configuration model is to be used, the objective function can assume one the following two forms:

1) For the fuel cell active model:

$$\min_{I_{d_i}} E_{H_2}(I_{d_i}) = \min_{I_{d_i}} \sum_{i=1}^{N} \frac{E_{M_i}}{\eta_{FC}(P_{FC_i}) \cdot \eta_{DCDC}} \tag{4.6}$$

2) For the parallel active hybrid model:

$$\min_{I_{d_i}} E_{H_2}(I_{d_i}) = \min_{I_{d_i}} \sum_{i=1}^{N} \frac{E_{M_i} + \frac{E_{SC,in_i}}{\eta_{DCDC}^2} - E_{SC,out_i}}{\eta_{FC}(P_{FC})} + E_{SC_N} \tag{4.7}$$

where N is the number of samples ($x_{lap} = x_N = N \cdot \Delta x$), P_{FC} is the FC power output and t_i is the time at x_i.

4.2 Optimization Strategy

One of the biggest deciding factors to achieve an efficient driving strategy is the optimization strategy (OS) used to determine where on the track and how much torque the motor produces. The optimization strategy is ultimately what determines the way in which the vehicle is controlled, i.e., maintaining an average velocity, accelerating or freewheeling, depending on the track section, etc.

After investigating and testing several optimization strategies common among SEM teams and finding that none satisfied all the desired objectives, a new unique optimization strategy was developed for the vehicle. The main objectives for the new strategy are:

1. Effectiveness: The resulting optimized driving strategy must be competitive;
2. Versatility: It can be used for any track;
3. Ready-to-use: The generated duty cycle can be directly used for the driving strategy;
4. Customizable: The number of "motoring" sections is defined by the user.

The new optimization strategy created, which will be referred to as "Adaptive Sections", independently defines the duty cycle for each section and also adapts the sections to the track by specifying the location, x_k, and length, d_k, of each of the "active" sections, as is shown in Figure 4.1.

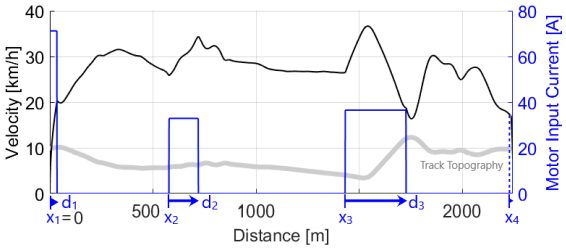

Figure 4.1 - Example of the Adaptive Sections strategy with four active sections (three motoring and one braking).

Since the number of active track sections, N, used is selected by the user, the general vector for the optimization strategy is represented by:

$$DCycle = [x_2, \dots, x_N, d_1, \dots, d_{N-1}, I_{d_1}, \dots, I_{d_N}] \tag{4.8}$$

and new constraints have to be added to the optimization problem of Section 4.1 to ensure that the N sections do not overlap and are all within the track range.

$$d_1 \in]0, x_2[\tag{4.9}$$

$$x_2 + d_2 < x_3 \tag{4.10}$$

$$\vdots$$

$$x_{N-1} + d_{N-1} < x_N \tag{4.11}$$

$$x_N \leq x_{lap} \tag{4.12}$$

4.2.1 Optimization Algorithm

Of all the algorithms tested from MATLAB's Optimization Toolbox, only the Genetic Algorithm (GA) and the Particle Swarm Optimization (PSO) showed real promise in solving the OP efficiently. However, due to its discrete nature, and the inability of MATLAB´s PSO algorithm to handle integer decision variables, the Mixed Integer GA (a GA variant for integer and mixed integer constrained optimization problems – also available in MATLAB's Optimization Toolbox), proved to be the best choice to solve the optimization problem of Section 4.1.

4.3 Powertrain Design

The design considerations of the powertrain and the driving strategy were defined according to the results of optimizations given by the models developed in this work.

The vehicle specifications used for the simulations are conservative and average compared to other SEM teams. The more important values are shown in Table 4.1.

Table 4.1 - Vehicle specifications.

Specifications	Value
Mass of the Vehicle[1]	100 kg
Mass of the Driver	70 kg
Wheelbase[1]	1.57 m
Track Front Wheels[1]	1.00 m
Track Rear Wheels[1]	0.80 m
Height of the CG[1]	0.343 m
Rear Wheel to CG[1]	0.587 m
Aerodynamic Drag Coefficient[1]	0.18
Frontal Area of the Vehicle[1]	0.9 m^2
Radius of the Wheel	0.275 m
Rolling Resistance Coefficient	0.002
DC-DC Converter Efficiency	90 %
Supercapacitor Efficiency	95 %
Gearbox Efficiency[2]	97 %
Chain Transmission Efficiency	90 %

[1] Values from a colleague's M.S. thesis [13];
[2] Dunkermotoren PLG 80 Planetary gearbox [8].

4.3.1 Fuel Cell Selection

The fuel cell selected for the vehicle is Horizon's 1 kW H-1000XP. It is a high efficiency system developed specifically for SEM Urban Concept vehicles that has proven itself with several vehicles achieving podium placement, including some wins. This system is most likely the best choice for the team since it is purposefully customized for the competition and also comes with every component needed to plug it on the vehicle and go.

4.3.2 Number of Active Sections

To select the number of active sections, the energy consumed by electric motor was optimized for three and up to eight active sections for two pre-selected BLDC motors. The result is shown in Figure 4.2.

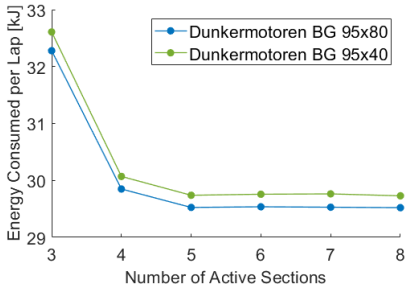

Figure 4.2 - Optimization of the number of active sections.

Analysing Figure 4.2, it is observed that four active sections reduces the number of power cycles used by 25% with a minimal increase in energy consumption of around 1%. For this reason, a driving strategy with four active sections is considered to be the best compromise between energy efficiency and fuel cell lifetime. Furthermore, since the model used does not take into account the transient of operation of the fuel cell, the fact that one less power cycle is used per lap can make the four active sections driving strategy the actual best option in terms of fuel efficiency.

4.3.3 BLDC Motor Selection

To select the best BLDC motor for the vehicle, the energy consumed per lap of three pre-selected BLDC motors was evaluated for transmission gear ratios ranging from 3:1 to 16:1. The data generated is plotted in the graph shown in Figure 4.3, where it can be observed that the Dunkermotoren BG 95X80 has the biggest potential for fuel efficiency for the majority of gear ratios. Concluding the selection.

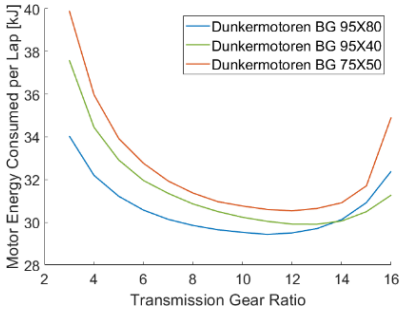

Figure 4.3 - Electrical energy consumption per lap of three BLDC motors, for different transmission gear ratios.

4.3.4 Powertrain Configuration and Transmission Gear Ratio Selection

Comparing the parallel active hybrid and the fuel cell active configurations for the BG 95X80 for transmission gear ratios ranging from 3:1 to 16:1 (Figure 4.4), it can be observed that both configurations generate very similar results in terms of fuel efficiency, with the parallel active hybrid producing slightly better results for an optimal transmission gear ratio of approximately 15:2. With this knowledge, and considering that the parallel active hybrid has a higher flexibility to respond to changing conditions in the track and/or during the race and that it isolates the fuel cell from the motor electric load, allowing it to work in more favourable conditions, the parallel active hybrid was the chosen configuration with a gear ratio of 15:2.

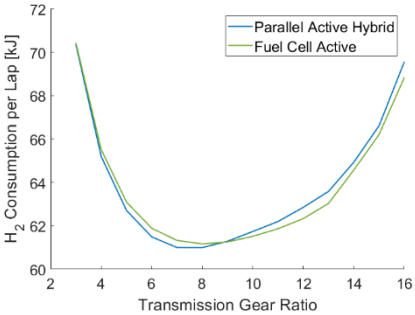

Figure 4.4 - Hydrogen consumption of the BG 95X80 for the two powertrain configurations, for different transmission ratios.

4.3.5 Regenerative Braking

After a deep analysis it was concluded regenerative braking might do more harm than good to the vehicle's global efficiency. The main reason is that, even for perfect conditions, the energy recuperated amounts to less than 3% of the total energy consumed by the electric motor and, in reality, this value should be considerably lower. The fact that this value is so low makes any slight drop in the vehicle performance caused by the regenerative braking or due to its installation not worth having it to begin with.

4.3.6 Supercapacitor Selection

To determine the minimum required capacity of the supercapacitor, its maximum and minimum charge levels were registered for the optimal run with the powertrain design selected so far. The evolution of the energy stored in the supercapacitor is shown in Figure 4.5, as well as the motor input and the fuel cell output power. It should be

noted that the SC charge level is measured in relation to a fictitious zero charge, which represents the initial state of the SC charge level on the starting line of the track.

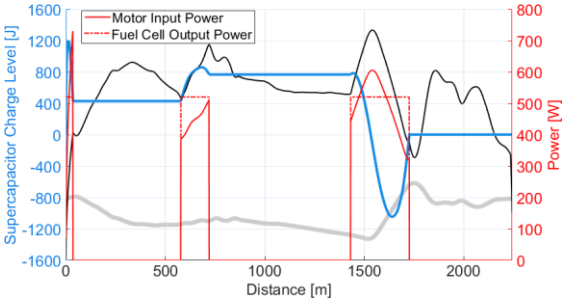

Figure 4.5 - Evolution of the supercapacitor charge level for the optimal driving strategy.

Note: The velocity (black line) was left for reference. It can be read by dividing the values on the right axis by 20.

The maximum and minimum charge levels of the supercapacitor during the run shown in Figure 4.5 are 1200.5 J and -1046.5 J, respectively. Knowing that 25% of the SC capacity is not used, the minimum required energy storage capacity of the SC is approximately 3000 J.

4.3.7 Number of Driving Wheels

To see if one-wheel drive is sufficient, the maximum traction and the tire drag caused by the turning of the front wheels to compensate for having only one rear driving wheel were evaluated for the optimal driving strategy.

Traction Verification: The maximum registered tractive force (Eq. (2.2)) in the run occurs on the starting line during acceleration and is around 100 N, which is considerably lower than the maximum traction available (Eq. (2.4)) of approximately 426 N for dry and 266 N for wet conditions (assuming asphalt or concrete).

Compensation Tire Drag: Having only one driving rear wheel causes the tractive force produced by the vehicle to not be in line with its the centre of mass, creating a momentum around the centre of mass that must be counterbalanced by slightly steering the front wheels .

The equilibrium for the vehicle, when the electric motor is powering the wheel, is described by:

$$M_t = \frac{t}{2} \cdot F_{xt} - b \cdot 2 \cdot F_t = 0 \qquad (4.13)$$

where F_t represent lateral force produced by the tires counteracting the turning moment M_t generated by the misaligned traction force F_{xt}.

Applying the cornering tire drag model with the lateral force calculated with equation (4.13), the energy lost due to the cornering effect of having one wheel drive is negligible, representing less than 0.06% of the total energy consumed by the electric motor. Hence, the author considers that the best solution for the drivetrain, considering the choice of motor and gear ratio, is a combination of a Dunkermotoren PLG 80 LB planetary gearbox with an 8:1 gear ratio for the first stage and, for the second, a roller chain connecting directly to the freehub (as in a bicycle) with a gear ratio of 15:16, making up the final transmission gear ratio of 15:2. This system considerably reduces the number shafts needed and, since the chain can withstand the vertical movements of suspension system, it avoids the use of universal joints and other complex mechanisms, making the powertrain simple, lightweight and very efficient.

A schematic of the envisioned drivetrain system is shown in Figure 4.6.

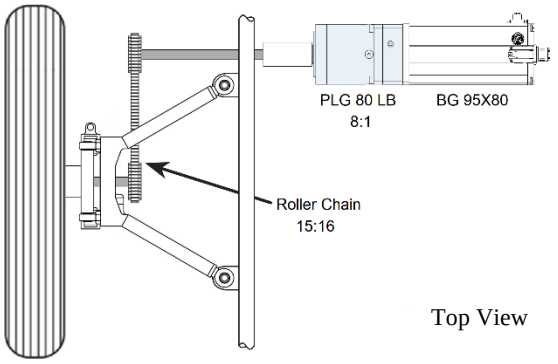

Figure 4.6 - The drivetrain system (suspension model from [14]).

4.4 Optimized Driving Strategy

The final estimated hydrogen consumption with the optimized driving strategy and powertrain design is 370.2 km/m^3 of hydrogen with a lap time of 310 seconds, 12.5 seconds less than the maximum time per lap to end the 8-lap race in exactly 43 minutes. This slightly higher lap time was chosen to give some margin for unforeseeable events or conditions during the race.

The result obtained means that, if the vehicle discussed in this work were to compete in the 2016 London edition of the SEM, and assuming it was able to perfectly execute the optimal driving strategy proposed, it would achieve a second place with a fuel efficiency slightly lower than the winning team's fuel efficiency of 389.3 km/m^3. In fact, that year the winning fuel efficiency was considerably higher than the other competing teams (39% higher than the second place), showing that expected fuel efficiency, which is just 5% lower than the winning team, would be an excellent result and, with further optimization of the vehicle, it could easily win that year's competition.

4.4.1 Energy Consumption Breakdown

The energy consumption of the vehicle can be broken-down into the various sources of energy loss as shown in the Sankey diagram of Figure 4.7.

It is interesting to note that, even though the average cruising speed of the vehicle is between 25 and 30 km/h, which is considerably lower than that of a regular road car, the aerodynamic drag is still the predominant resistive force acting on the vehicle, even considering that the body shape is highly aerodynamic. This shows the importance that aerodynamics have on the fuel consumption and serves as a warning that every change to the vehicle's body surface must be carefully studied to avoid worsening the aerodynamic drag.

After the aerodynamic drag, the resistance caused by the tires under "normal" rolling conditions and when cornering (approximately 11% of the total tire drag), is by far the largest cause of energy loss. Furthermore, special attention should be given to the tires and the steering system to ensure that everything is perfectly lined up and working flawlessly because, if any misalignment or tire wobbling occurs, the rolling resistance increases significantly, easily surpassing the energy loss due to aerodynamics and possibly even ruining the run.

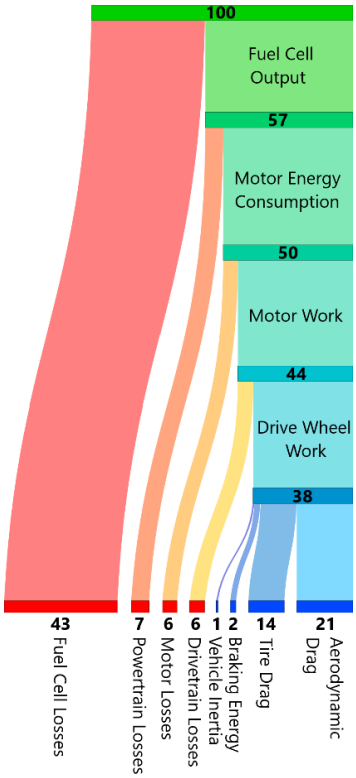

Figure 4.7 - Vehicle energy consumption breakdown.

4.5 Sensitivity Analysis

In this section, a quick analysis of the impact that changes to certain characteristics of the vehicle have on the energy consumption will be done for the powertrain design selected in Section 4.3. This study aims to highlight where the major efforts for the improvement of the vehicle should be focused on and also points out possible areas that are not worth investing in.

4.5.1 Vehicle Mass

As expected, the fuel consumption increases linearly with the vehicle mass (Figure 4.8). For a lighter vehicle with 70 kg the fuel consumption would decrease 7.7% and for a heavier one with 135 kg it would increase 9.5%. In other words, the amount of hydrogen consumed is expected to increase 2.7% with each 10 kg increment to the mass of the vehicle.

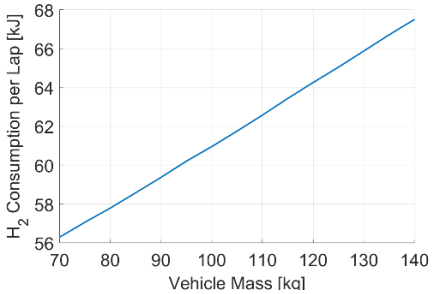

Figure 4.8 - Sensitivity of the fuel consumption to vehicle mass.

4.5.2 Quality of the Tires

One of the reoccurring themes that was encountered during the research of ultra-efficient vehicles is the major role that the tires have on fuel efficiency. It was even found that many of the vehicles that have reached podium placement or even won the SEM use the same specially designed Michelin tires.

The sensitivity analysis for the rolling resistance of the tires (Figure 4.9) clearly reveals why the tires are so important. A mere increase of the rolling resistance from 0.002 to 0.004 causes an increase in fuel consumption of 27%. It should be noted that 0.004 is a very low value of rolling resistance for a tire, roughly half than that of the best energy-efficient car tires available on the market.

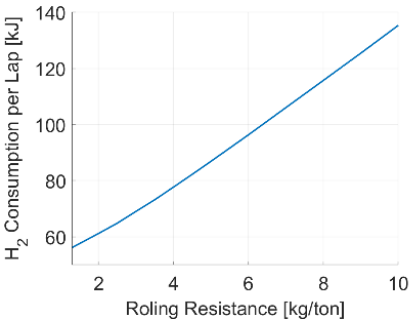

Figure 4.9 - Sensitivity of the fuel consumption to the tires rolling resistance coefficient.

4.5.3 DC-DC Converters Efficiency

Compared to the assumed converter efficiency of 90%, an increase in efficiency to 96% (+6%) would result in a reduction in fuel consumption of 7.5%, while a reduction to 84% (-6%) results in an increase in fuel consumption of 9.7% (Figure 4.10). This shows the importance of keeping the converters efficiency as high as possible, giving priority to the main DC-DC converter that is right after the fuel cell, since about 90% the FC energy output goes through it directly into the electric motor.

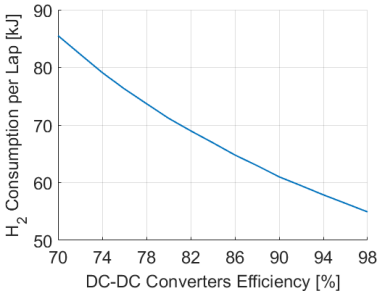

Figure 4.10 - Sensitivity of the fuel consumption to the efficiency of the DC-DC converters.

4.5.4 Supercapacitor Efficiency

Figure 4.11 shows that the efficiency of the SC plays a minor role in the total fuel efficiency of the vehicle. This is because only about 10% of the total energy output of the FC goes to the supercapacitor. For example, comparing a supercapacitor with an efficiency of 80% with one 98% efficient, the fuel consumption reduction is only 2%.

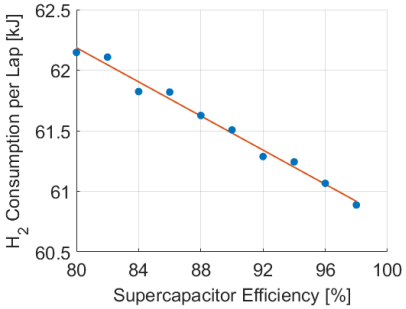

Figure 4.11 - Sensitivity of the fuel consumption to the efficiency of the supercapacitor.

4.5.5 Aerodynamic Drag Coefficient

The range of aerodynamic drag coefficients chosen span from 0.14, which is the best theoretical value that can be achieved by the TFC vehicle developed in [13], to a mediocre 0.3, easily achieved by many production cars.

The analysis (Figure 4.12) shows that the fuel consumption increases approximately 14.5% per 0.05 increase in the aerodynamic drag coefficient, which goes to show how important it is to keep it as low as possible to be able to compete with other teams in terms of efficiency.

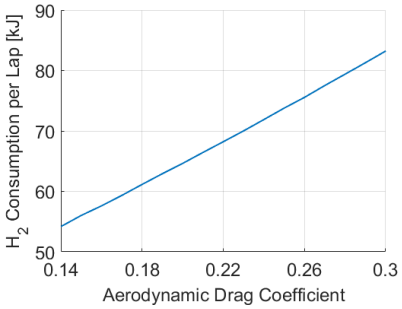

Figure 4.12 - Sensitivity the fuel consumption to the aerodynamic drag coefficient.

5 Conclusions

After the study and design of the vehicle's powertrain system and driving strategy, the conclusions that stand out the most are listed below:

1. The work developed in this article brings a new perspective to the development of high fuel efficient vehicles by combining the design and component selection process with the development of the driving strategy;

2. The developed method ensures that the powertrain is a perfect match for the driving strategy, which enables the vehicle to reach maximum fuel efficiency;

3. The parallel active hybrid is the most efficient configuration and has a higher flexibility to respond to changing conditions in the track and/or during the race;

4. Regenerative braking should not be used since it is estimated to be close to 1% of the energy consumed by the electric motor and, in using it, the effect on the fuel efficiency might be the opposite of the desired;

5. One rear driving wheel was found to be the best drivetrain architecture because it is much simpler, cheaper, easier to build and maintain as well as being the most efficient configuration;

6. The tire road traction available at just the one rear wheel is estimated to be more than sufficient for both dry and wet conditions and no tire slip is expected to occur;

7. Considering that the vehicle specifications selected are conservative, the result of the optimization strategy proved to be excellent, at just 5% lower than the result that overwhelmed the competition SEM London 2016;

8. The study done on the sensitivity concluded that the main factors that influence the fuel efficiency are the rolling resistance of the tires, the efficiency of the DC-DC converter and the aerodynamic drag coefficient;

9. Finally, with the sensitivity analysis in mind, it was concluded that if the values for any of the three main factors that influence the fuel efficiency were slightly improved, the TFC vehicle could have easily surpassed the fuel efficiency of the winner of SEM London 2016 hydrogen urban concept class.

Acknowledgements

The author would like to thank Prof. João Dias and Prof. Rui Costa Neto for all the motivation and unwavering support given throughout the development of this work. Also, a special thanks to all members of Técnico Fuel Cell, it was a wonderful experience working side-by-side with you all in the pursuit of a greener, more efficient Future.

References

[1] A. Emadi *et al.*, *Advanced Electric Drive Vehicles*. New York: Taylor & Francis Group LLC, 2015.

[2] J. J. Santin *et al.*, *The World's Most Fuel Efficient Vehicle: Design and Development of PAC-Car II*. Zürich: VDF Hochschulverlag AG an der ETH Zürich, 2007.

[3] P. Yedamale and Microchip Technology Inc., "Brushless DC (BLDC) Motor Fundamentals." Microchip Technology Inc., 2003.

[4] K. Krykowski, Z. Gałuszkiewicz, P. Gałuszkiewicz, J. Hetmańczyk, and D. Całus, "High-speed Permanent Magnet Brushless DC Motors, Properties and Prospective Applications," *Prz. Elektrotechniczny*, vol. 95, no. 8, pp. 139–145, Aug. 2019, doi: 10.15199/48.2019.08.30.

[5] L. Nakuçi and A. Spahiu, "Saving Energy by Replacing IM with BLDC Motor in Fan Application," *European Journal of Electrical Engineering and Computer Science*, vol. 2, no. 5, Aug. 2018.

[6] S. Derammelaere, M. Haemers, J. De Viaene, F. Verbelen, and K. Stockman, "A quantitative comparison between BLDC, PMSM, brushed DC and stepping motor technologies," *2016 19th Int. Conf. Electr. Mach. Syst.*

[7] K. Krykowski and J. Hetmańczyk, "Constant Current Models of Brushless DC Motor," *Electr. Control Commun. Eng.*, vol. 3, no. 1, pp. 19–24, Sep. 2013, doi: 10.2478/ecce-2013-0010.

[8] Dunkermotoren GmbH, "Motors | Gearboxes Controllers | 2020 Catalogue." Bonndorf, Germany, pp. 78–79, 2020.

[9] T. Verstraten, R. Furnémont, G. Mathijssen, B. Vanderborght, and D. Lefeber, "Energy Consumption of Geared DC Motors in Dynamic Applications: Comparing Modeling Approaches," *IEEE Robotics and Automation Letters*, vol. 1, no. 1, pp. 524–530, Jan. 2016.

[10] Shell Eco-marathon, "Shell Eco-marathon 2021 Official Rules, Chapter 1." 2020.

[11] A. Kuperman and I. Aharon, "Battery-ultracapacitor hybrids for pulsed current loads: A review," *Renew. Sustain. Energy Rev.*, vol. 15, no. 2, pp. 981–992, Feb. 2011, doi: 10.1016/j.rser.2010.11.010.

[12] Horizon Educational, "User Manual H-1000XP Fuel Cell System." Aug. 05, 2013.

[13] C. A. Mesquita, "Projecto de um veículo eléctrico de competição movido a hidrogénio," M.S. thesis, Instituto Superior Técnico, Univ. Lisboa, Lisboa, 2021.

[14] P. D. de Matos, "Metodologias Integradas de CAD , CAE e PDM para o Projeto de um Veículo de Competição," M.S. thesis, Instituto Superior Técnico, Univ. Lisboa, Lisboa, 2020.